Molecular origin of the difference in the HOH bend of the IR spectra between liquid water and ice

ARTICLE *in* THE JOURNAL OF CHEMICAL PHYSICS · FEBRUARY 2013

Impact Factor: 2.95 · DOI: 10.1063/1.4789951 · Source: PubMed

3 AUTHORS, INCLUDING:

Sotiris S Xantheas
Pacific Northwest National Laboratory
178 PUBLICATIONS **7,759** CITATIONS
SEE PROFILE

Shinji Saito
Institute for Molecular Science
74 PUBLICATIONS **3,348** CITATIONS
SEE PROFILE

Molecular origin of the difference in the HOH bend of the IR spectra between liquid water and ice

Sho Imoto,[1] Sotiris S. Xantheas,[2] and Shinji Saito[1,3,a)]
[1]*The Graduate University for Advanced Studies, Myodaiji, Okazaki, Aichi 444-8585, Japan*
[2]*Physical Sciences Division, Pacific Northwest National Laboratory, 902 Battelle Boulevard, P.O. Box 999, MS K1-83, Richland, Washington 99352, USA*
[3]*Department of Theoretical and Computational Molecular Science, Institute for Molecular Science, Myodaiji, Okazaki, Aichi 444-8585, Japan*

(Received 23 November 2012; accepted 17 January 2013; published online 6 February 2013)

The intensity of the HOH bend in the infrared (IR) spectrum of ice is significantly smaller than the corresponding one in liquid water. This difference in the IR intensities of the HOH bend in the two systems is investigated using Molecular Dynamics (MD) simulations with the flexible, polarizable, *ab initio* based TTM3-F model for water, a potential that correctly reproduces the experimentally observed increase of the HOH angle in liquid water and ice from the water monomer value. We have identified two factors that are responsible for the difference in the intensity of the HOH bend in liquid water and ice: (i) the decrease of the intensity of the HOH bend in ice caused by the strong anti-correlation between the permanent dipole moment of a molecule and the induced dipole moment of neighboring hydrogen bond acceptor molecules, and (ii) the weakening of this anti-correlation by the disordered hydrogen bond network in liquid water. The presence of the anti-correlation in ice is further confirmed by *ab initio* electronic structure calculations of water pentamer clusters extracted from the trajectories of the MD simulations with the TTM3-F potential for ice and liquid water. [http://dx.doi.org/10.1063/1.4789951]

I. INTRODUCTION

Water is the most abundant liquid on earth and has several anomalous thermodynamic and dynamical properties,[1] many of which have been attributed to its fleeting three-dimensional hydrogen bond (HB) network.[2] There are many experimental and theoretical studies of the HB in water. For example, the infrared (IR) spectrum of liquid water has been extensively studied because it is sensitive to the underlying HB structures.[3–5] The IR spectrum of liquid water consists of the intermolecular motions between 0 and 1000 cm^{-1}, a band centered at 1600 cm^{-1} arising from the HOH bend, and a broad band between 3000 and 4000 cm^{-1} corresponding to the OH stretching vibrations. It is well known that both the frequency and the intensity of the OH stretching vibrations are sensitive to the local HB environment. Strong HBs result in redshifted transition frequencies, as is the case, for instance, for the OH stretching vibrations in ice when compared to liquid water. The dynamics of the OH stretch have been studied using ultrafast nonlinear spectroscopy, e.g., two-dimensional (2D) IR spectroscopy. The 2D IR spectra revealed that the frequency correlation of the OH stretch in liquid D_2O and the OD stretch in liquid H_2O is associated with a rapid sub 100 fs decay, an underdamped oscillation of 130 fs induced by HB stretch, and a slow decay with the time constant of ∼1 ps.[6–9] The 2D IR spectra of the OH stretch in neat water display a loss of frequency correlation on a 50 fs time scale and that of neat ice display a sub 100 fs time scale randomization of the transition dipole.[10,11]

It is known that the bend mode in the IR spectrum of liquid water shows a redshift with increasing temperature, i.e., the temperature-dependence of the IR spectrum of the HOH bend is opposite to that of the OH stretch.[4] In addition, the IR spectrum of the HOH bend of ice is weaker and broader than that of liquid water.[12] The time scale of the energy relaxation of the HOH bend in neat liquid water and aqueous solution of ions at room temperature has been measured using pump-probe experiments.[13–16] The vibrational relaxation of the HOD bend in liquid D_2O has been also experimentally studied.[17] The details of the fluctuation and dynamics of the HOH bend are, however, still not well understood.

Theoretical studies of the HOH bend have also been limited. However, the energy relaxation dynamics of the HOH bend have been recently examined theoretically. Hynes and co-workers studied the time scale and pathway of the HOH bend relaxation mechanism by using the classical non-equilibrium MD simulations.[18,19] Miguel and co-workers investigated the quantum effects on the energy relaxation of the HOH bend and the HOD bend via quantum/classical hybrid MD simulations.[20,21] Kandratsenka and co-workers reported the energy relaxation pathway of the OD stretch in D_2O via the HOD bend employing classical non-equilibrium MD simulations.[22] The fact that theoretical studies of the HOH bend in liquid water and ice using simple interaction potentials are scarce can be, in part, attributed to the fact that these simple models predict the opposite effect, viz., the *decrease* in the value of the average HOH bend angle from the monomer to liquid water and ice in contrast to the *increase* that has been observed either experimentally or obtained from first principles simulations.[23–28] It is also known that the IR

a)Electronic mail: shinji@ims.ac.jp.

intensity of the HOH bend is overestimated by simple interaction potentials for water.

This is not, however, the case for the Thole-type models (TTM), previously introduced by Xantheas and co-workers, who showed that the intramolecular charge transfer is essential for reproducing the experimentally observed increase of the HOH angle in the condensed phase with respect to the monomer.[29] When this intramolecular charge transfer was "turned off," the HOH angle in ice and liquid water was smaller than the monomer value, like in all previous fixed charge models. The flexible, polarizable transferable model TTM2.1-F,[30] which uses the *ab initio*-based dipole moment surface of the gas phase monomer, was shown to properly describe both the increase and associated IR intensity of the HOH bend in the condensed phase.[29,30] The latest version 3.0 of the TTM family of potentials (TTM3-F)[31] was shown to reproduce the IR spectra[31–34] and other properties of the liquid[31,35–37] more accurately.

In this study we used the TTM3-F water model potential to analyze the obtained molecular level insight into the difference between the IR peak band structure of the HOH bend of ice and liquid water. The theoretical background is outlined in Sec. II. The details of classical MD simulations and subsequent analysis for the clusters via *ab initio* electronic structure calculations are described in Sec. III. The results are presented and discussed in Sec. IV with final conclusions drawn in Sec. V.

II. METHODS

The IR spectrum is related to the fluctuation of the total dipole moment of the system. When the harmonic quantum correction is applied to the classical IR spectra to satisfy the detailed balance condition, the IR spectrum is expressed as

$$I(\omega) = \frac{4\pi\omega^2}{3Vck_BT} \cdot \frac{1}{2\pi} \int dt\, e^{-i\omega t} \langle \delta\mathbf{M}(t)\delta\mathbf{M}(0)\rangle. \quad (1)$$

Here, V, T, and $\delta\mathbf{M}$ are the volume, temperature, and the fluctuation of the total dipole moment of the system, c is the speed of light, and k_B is the Boltzmann constant. The total dipole moment is expressed as the sum of the permanent and interaction-induced dipole moments,

$$\mathbf{M} = \mathbf{M}^{\text{perm}} + \mathbf{M}^{\text{ind}}. \quad (2)$$

Thus, the IR spectrum is the contribution of three terms, viz.,

$$\begin{aligned} I(\omega) &= I^{\text{perm}}(\omega) + I^{\text{ind}}(\omega) + I^{\text{cross}}(\omega) \\ &\propto \int dt e^{-i\omega t} \langle \delta\mathbf{M}^{\text{perm}}(t)\delta\mathbf{M}^{\text{perm}}(0)\rangle \\ &+ \int dt e^{-i\omega t} \langle \delta\mathbf{M}^{\text{ind}}(t)\delta\mathbf{M}^{\text{ind}}(0)\rangle \\ &+ \int dt e^{-i\omega t} \langle \delta\mathbf{M}^{\text{perm}}(t)\delta\mathbf{M}^{\text{ind}}(0) \\ &+ \delta\mathbf{M}^{\text{ind}}(t)\delta\mathbf{M}^{\text{perm}}(0)\rangle. \end{aligned} \quad (3)$$

Hereafter, we will refer to these three terms in the right-hand side of Eq. (3) as the *permanent*, *induced*, and *cross terms*, respectively.

The instantaneous normal mode approach when employed to obtain $\mathbf{M}(t)$ via the lowest-order expansion yields[38]

$$\mathbf{M}(t) = \mathbf{M}(0) + \sum_\alpha \left.\frac{\partial\mathbf{M}}{\partial Q_\alpha}\right|_{t=0} Q_\alpha(t), \quad (4)$$

where $Q_\alpha(t)$ is the normal mode α given by

$$Q_\alpha(t) = Q_\alpha(0)\cos(\omega_\alpha t) + \frac{V_\alpha(0)}{\omega_\alpha}\sin(\omega_\alpha t). \quad (5)$$

Here, $V_\alpha(0)$ is the initial velocity of the normal mode α. By substituting Eq. (4) into Eq. (1), the IR spectrum is expressed as

$$I(\omega) = \frac{2}{3Vc}\left\langle \sum_\alpha \left|\frac{\partial\mathbf{M}}{\partial Q_\alpha}\right|^2 \delta(\omega-\omega_0)\right\rangle. \quad (6)$$

The angle bracket denotes the averaging over the thermal distribution of the ice or liquid water configurations. As a result, the permanent, induced, and cross terms in the normal mode approximation are given by

$$I^{\text{perm}}(\omega) \propto \left\langle \sum_\alpha \left|\frac{\partial\mathbf{M}^{\text{perm}}}{\partial Q_\alpha}\right|^2 \delta(\omega-\omega_\alpha)\right\rangle, \quad (7)$$

$$I^{\text{ind}}(\omega) \propto \left\langle \sum_\alpha \left|\frac{\partial\mathbf{M}^{\text{ind}}}{\partial Q_\alpha}\right|^2 \delta(\omega-\omega_\alpha)\right\rangle, \quad (8)$$

$$I^{\text{cross}}(\omega) \propto 2\left\langle \sum_\alpha \frac{\partial\mathbf{M}^{\text{perm}}}{\partial Q_\alpha}\cdot\frac{\partial\mathbf{M}^{\text{ind}}}{\partial Q_\alpha}\delta(\omega-\omega_\alpha)\right\rangle. \quad (9)$$

III. COMPUTATIONAL DETAILS

A. Molecular dynamics and normal mode analysis

We used the TTM3-F interaction potential, a transferable, flexible, polarizable model to describe the intra- and inter-molecular interactions in liquid water and ice. Although the details of TTM3-F potential are presented in Ref. 31, we briefly account for some of its salient features here. The intramolecular interaction and charge transfer scheme of the TTM3-F potential is based on the adaptation of the high level *ab initio* gas phase water monomer potential and dipole moment surface of Partridge and Schwenke[39] to account for the liquid environment. The potential has four interaction sites that are used to describe the intermolecular interaction. The oxygen-oxygen interaction is described by a Buckingham exponential-6 potential. A positive charge is placed on each hydrogen atom and a negative charge and an isotropic point dipole moment are placed on the M site located on the bisector of the HOH angle. The Thole-type damping function is employed for the treatment of the electrostatic interactions.[40] In the analysis with the TTM3-F potential, the permanent and induced dipole moments are defined as the dipole moment originating from the point charges and the point dipole moment, respectively.

We carried out classical MD simulations of periodic supercells of liquid water and ice Ih under the constant volume and energy conditions.[41] The MD simulations of liquid water were carried out at a temperature of 300 K using a supercell of

125 water molecules with a density of 1.0 g/cm^3. The resultant dielectric constant calculated with the TTM3-F potential is 67.7. We averaged the results over eight trajectories, each of which had a length of 500 ps. The MD simulations of ice Ih were performed at a temperature of 230 K with a rectangular supercell of 96 molecules with dimensions $L_x \times L_y \times L_z = 13.5 \times 15.6 \times 14.7$Å^3 containing $3 \times 2 \times 2$ unit cells and a density of 0.92 g/cm^3. The analysis of the results for ice was performed over one hundred trajectories, which started from different initial configurations. The length of each trajectory for the ice simulations was 50 ps. For both the liquid water and ice simulations, periodic boundary conditions were employed and the long-range electric interactions were calculated by using the Ewald sum. Equations of motion were integrated using the velocity-Velret algorithm with the time step of 0.05 fs. The induced dipole moment was obtained iteratively at each step.

Normal modes for ice and liquid water were obtained using configurations taken from the MD trajectories. We used a total of 300 and 200 configurations for ice and liquid water, respectively. We also performed normal mode analysis for ∼3000 pentamer clusters randomly selected from the MD trajectories of liquid water and ice.

B. *Ab initio* calculations

The total dipole moment of each molecule in a pentamer cluster was calculated using the distributed multipole analysis (DMA), in which the *n*th multipole expansion is obtained via spherical harmonics.[42] The advantage of using DMA is that both the out of plane and in-plane components of the induced dipole moments can be reproduced. We defined the total dipole moment of each molecule as a sum of the dipole moment calculated from the point charges and point dipoles. We also defined the permanent and induced dipole moments of each molecule as the dipole moment of the water molecule given by Partridge and Schwenke in Ref. 39 and the difference between the total dipole moment and the permanent dipole moment, respectively. The DMA was carried out using the GDMA 2.2 program.[43] All *ab initio* calculations for the pentamer clusters extracted from the MD trajectories generated with the TTM3-F potential were carried out at the MP2 level of theory with the aug-cc-pVDZ basis set[44] using the GAUSSIAN09 package.[45] The positions of only the hydrogen atoms of the central molecules in each pentamer cluster were optimized. Overall, we performed MP2/aug-cc-pVDZ calculations on ∼600 configurations for both ice and liquid water. The dipole derivatives were evaluated by using a 4-point differentiation formula.

IV. RESULTS AND DISCUSSION

Figure 1 shows the IR spectra of ice (blue line) and liquid water (red line) obtained with TTM3-F potential. Intermolecular translational and rotational motions are seen at 200 cm^{-1} and 600 cm^{-1} as broad bands in liquid water, whereas two distinct peaks with the corresponding maxima approximately at 200 cm^{-1} and 800 cm^{-1} are obtained for ice. The peak

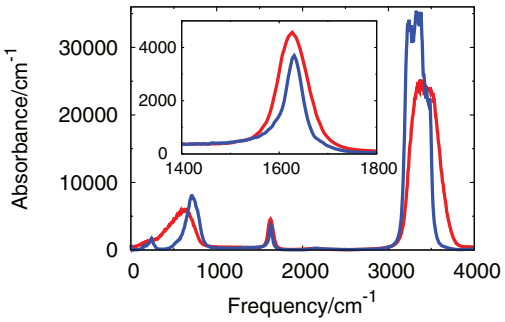

FIG. 1. IR spectra of ice (blue) and liquid water (red) obtained from MD simulations with the TTM3-F potential. The inset shows the magnification of the HOH bend region.

at 60 cm^{-1}, arising from the low frequency translational motion, is significantly suppressed in ice, whereas it appears as a shoulder in the spectra of liquid water in agreement with the experimental results.[3,5]

The permanent, induced, and cross terms defined in Eq. (3) are shown in Fig. 2. The IR spectrum in the intermolecular region mainly arises from the permanent term both in ice and in liquid water. Although the spectrum shows a shoulder around 200 cm^{-1} due to the cross term, the intensity of the shoulder is smaller than the experimental results. Previous analysis of this feature via Car-Parrinello MD (CPMD) simulations suggests that the shoulder is related to the intermolecular charge transfer.[46]

The peak maxima of the OH stretch are centered at 3340 cm^{-1} in ice and at 3430 cm^{-1} in liquid water, respectively. The peak of the OH stretch in ice is narrow and red-shifted compared to that in liquid water due to the less heterogeneous, stronger HBs in ice. It has been previously suggested that the calculated OH stretching band consists of three peaks due to the intermolecular vibrational coupling.[47] The intensity of the OH stretch in liquid water is the same as that reported in Ref. 34. It is larger than the one reported earlier[31] because a longer time interval was used in the calculation of the dipole correlation function in Ref. 31. Since the permanent and cross terms of the OH stretch in ice are slightly larger than those in liquid water, the IR intensity of the OH stretch in ice is larger than that in liquid water as seen in Figs. 2(a) and 2(b).

The IR spectra of the HOH bend of ice and liquid water are shown in the inset of Fig. 1. The calculated IR intensity of the HOH bend in ice is weaker than that in liquid water in agreement with the experimental result,[4] although the calculated width of the HOH bend in ice is narrower than the experimental result. Figures 2(c) and 2(d) show the three terms of the HOH bend in ice and liquid water. In liquid water, the contributions of the induced and cross terms are very small and, thus, the IR intensity of the HOH bend mainly arises from the permanent term. On the other hand, the cross term in ice shows a large negative value, though the intensity of the permanent term in ice is larger than that in liquid water. As a result, the total IR intensity of the HOH bend in ice is weaker than that in liquid water.

The density of states (DOS) calculated from the velocity-velocity correlation function and normal mode analysis is shown in Figs. 3(a) and 3(b). The DOS of ice calculated from

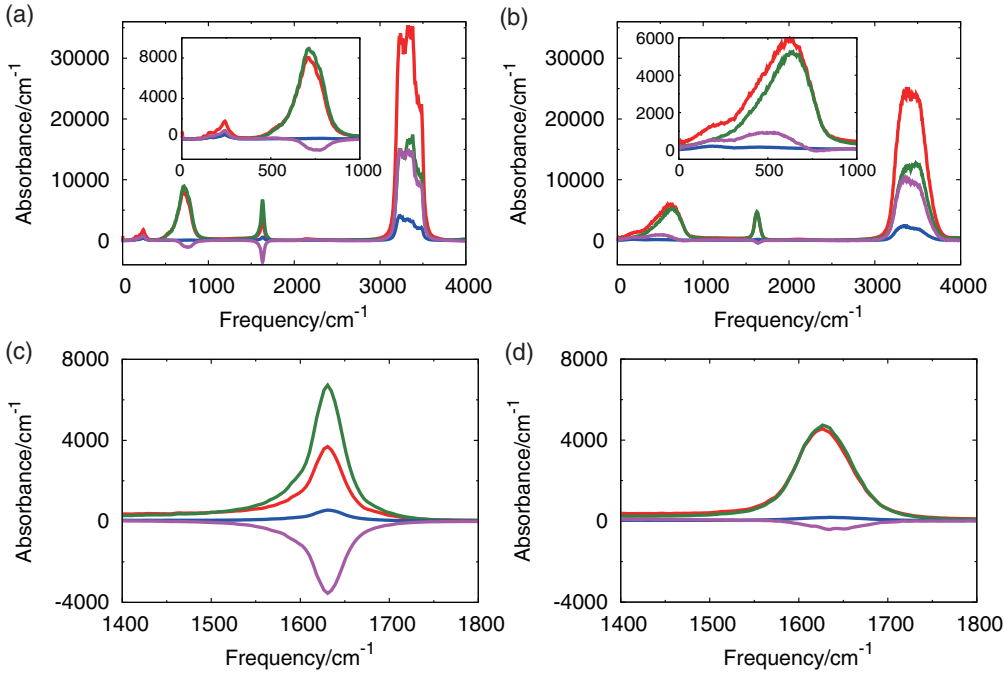

FIG. 2. IR spectra (red) and its components arising from the permanent (green), induced (blue), and cross term (purple) of (a) ice and (b) liquid water obtained from the MD simulations. The inset shows the magnifications in the intramolecular region. Panels (c) and (d) are magnifications of the HOH bend region in ice and liquid water, respectively.

the velocity-velocity correlation function shows structures at the OH stretch and intermolecular regions, whereas the one calculated from the normal mode analysis exhibits structureless inhomogeneous broad bands. The DOS of the HOH bend calculated from the normal mode analysis also shows inhomogeneous broadening that is about two times broader than that calculated from the velocity-velocity correlation function as the OH stretch.

The inverse participation ratio (IPR)[48] is shown in Fig. 3(c). The IPR of the mode α is given by

$$R_\alpha = \frac{1}{\sum_{I=1}^{N_{\mathrm{mol}}} \left[\sum_{i\in I} U_{\alpha i}^2\right]^2}. \tag{10}$$

Here, **U** is the normal mode transformation matrix and N_{mol} is the total number of the molecules. If a normal mode is localized on a single molecule, i.e., the eigenvector elements of only one molecule are nonzero, the IPR of the mode would be equal to 1. On the other hand, for a completely delocalized mode, the IPR of the mode is equal to N_{mol}. The IPRs of the HOH bend in ice and liquid water are 9 and 11, respectively, whereas those of the OH stretch in ice and liquid water are 8 and 5, respectively. The range of numbers for liquid water obtained via the IPR analysis is consistent with the estimates reported earlier using a different metric,[33] suggesting that a number of ∼10 neighbors is sufficient to reproduce the electric field along the OH bond and fully recover the structure of the OH stretching band with respect to the bulk spectra of liquid water. When the molecule with the largest IPR of a HOH bend (OH stretch) mode is defined as the central molecule of the mode, the average contribution of this central molecule to the HOH bend amounts to 0.43 and 0.38 for ice and liquid water, respectively. The cumulated contribution of the HOH bend within the first hydration shell of the central molecule amounts to 0.52 and 0.48 for ice and liquid water, respectively. The corresponding contributions of the central molecule to the OH stretch are 0.48 and 0.59, and the cumulated contribution within the first hydration shell of the central molecule of the OH stretch is 0.70 and 0.84 for ice and liquid water, respectively. The HOH bend is therefore more delocalized than the OH stretch.

Figures 4(a) and 4(b) show the contributions of the permanent, induced, and cross terms in the IR spectra of ice and liquid water calculated from the normal mode analysis. The IR spectra calculated from the normal mode analysis are broader than those obtained via the dipole correlation function from the MD simulations because of the absence of motional narrowing in the former. Similar to the results of the MD simulation, the IR intensity of the HOH bend in liquid water arises almost exclusively from the permanent term as the contributions of the induced and cross terms are small. In contrast, the cross term of the HOH bend in ice (like the case for liquid water) is negative. Thus, the total IR intensity of the HOH bend in ice is weaker than that of the permanent term in ice and also the IR intensity of the bend in liquid water, similar to the result obtained from the MD simulations.

We have examined the decrease in the IR intensity of the HOH bend of ice using normal mode analysis. To clarify the origin of the negative contribution of the cross term in the IR spectrum of ice, the radial component of the cross term was analyzed by using the following equation:

$$I_\alpha(r) = \left\langle \sum_j \left\{ \frac{\partial \mu_i^{\mathrm{perm}}}{\partial Q_\alpha} \cdot \frac{\partial \mu_j^{\mathrm{ind}}}{\partial Q_\alpha} + \frac{\partial \mu_i^{\mathrm{ind}}}{\partial Q_\alpha} \cdot \frac{\partial \mu_j^{\mathrm{perm}}}{\partial Q_\alpha} \right\} \delta(r - r_{ij}) \right\rangle, \tag{11}$$

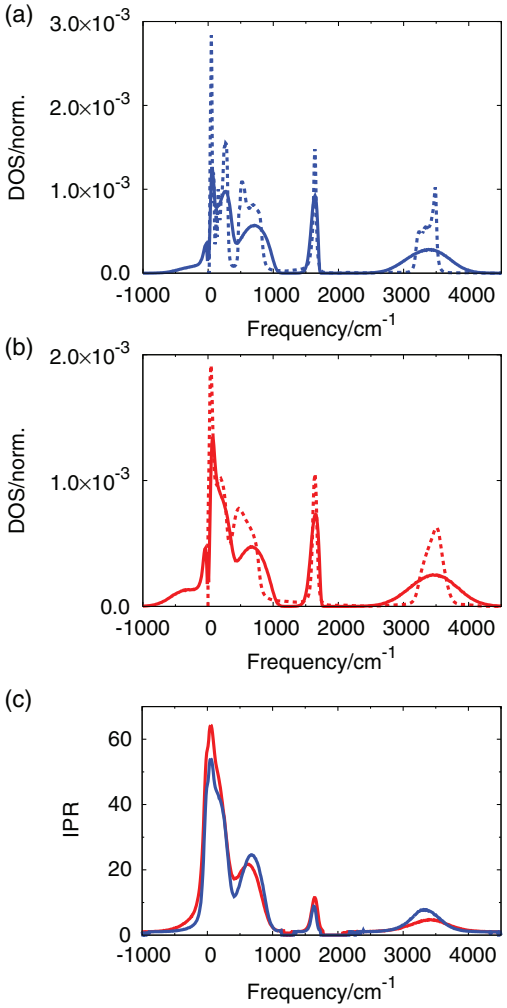

FIG. 3. Density of states (DOS) of (a) ice and (b) liquid water obtained from velocity-velocity correlation function (dotted line) and normal mode analysis (solid line). The DOS is normalized by the integrated values. (c) Inverse participation ratio (IPR) of ice (blue) and liquid water (red).

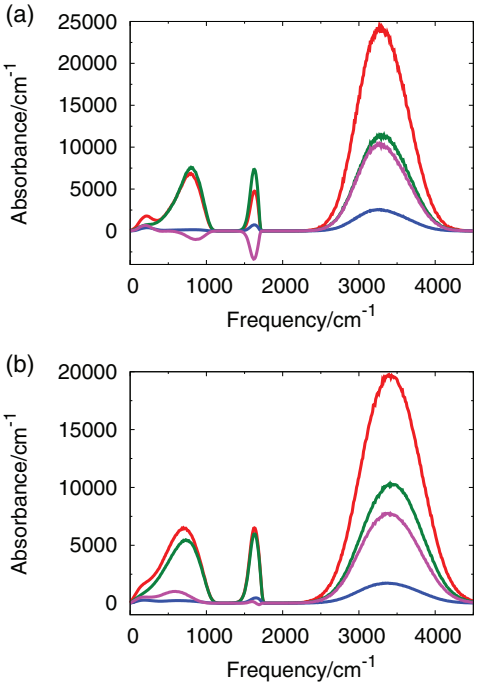

FIG. 4. IR spectra (red) and its components arising from the permanent (green), induced (blue), and cross term (purple) of (a) ice and (b) liquid water obtained from the normal mode approximation.

where α is a mode, i.e., HOH bend or OH stretch, i is the central molecule of the mode α, j is a molecule located at distance r from molecule i, and μ_k^{perm} and μ_k^{ind} are the permanent and induced dipole moments of molecule k. The first and second terms of Eq. (11) for the HOH bend and the OH stretch together with the oxygen-oxygen radial distribution function are presented in Fig. 5. Since the second term of Eq. (11) (dotted lines in Figs. 5(b) and 5(c)) is very small compared with the first term (solid lines in Figs. 5(b) and 5(c)) for both the HOH bend and the OH stretch, we will thereafter consider only the first term of Eq. (11) in our analysis. As seen in Fig. 5(b), the negative correlation for the HOH bend in ice mainly arises from that between the permanent dipole moment of a given central molecule and the induced dipole moment in the first hydration shell of that molecule. Indeed, the correlation between the permanent dipole moment of the central molecule and the induced dipole moment of its second and outer hydration shells is negligible in ice. In contrast, in liquid water the negative correlation in the first hydration shell is weakened because of the disordered orientation. In addition, the permanent dipole moment of the central molecule and the induced dipole moment of its second and outer hydration shells have a positive correlation in liquid water. As a result, the cross term of the HOH bend is further weakened in liquid water.

The radial component of the cross term for the OH stretch is shown in Fig. 5(c). Contrary to the negative correlation found for the HOH bend, the correlation between the permanent dipole moment of the central molecule and the induced dipole moment in its first hydration shell is positive for the OH stretch. Additionally, the correlation between the permanent dipole moment and the induced dipole moment of its second and outer hydration shells is negligible. As was the case for the correlation in the HOH bend, the correlation between the permanent dipole moment of the central molecule and the induced dipole moment of its first hydration shell in liquid water is smaller than the one in ice. It is noted that similar negative and positive intermolecular correlations for the HOH bend and OH stretch modes were also reported during previous CPMD simulations.[49]

Figure 6 shows the distribution of the magnitude of the correlation between the permanent dipole moment of the central molecule and the induced dipole moment of the molecule in its first hydration shell. We have defined the HB acceptor and donor molecules as the nearest molecule from the hydrogen atoms of the central molecule and the two nearest molecules from the oxygen atom of the central molecule, respectively. The correlation between the permanent dipole moment of the central molecule and the induced dipole moment of its HB donor molecule is small since the induced dipole moment of the HB donor molecule is insensitive to the bend motion of the central molecule as shown in the inset of Fig. 6. The anti-correlation between the permanent dipole moment

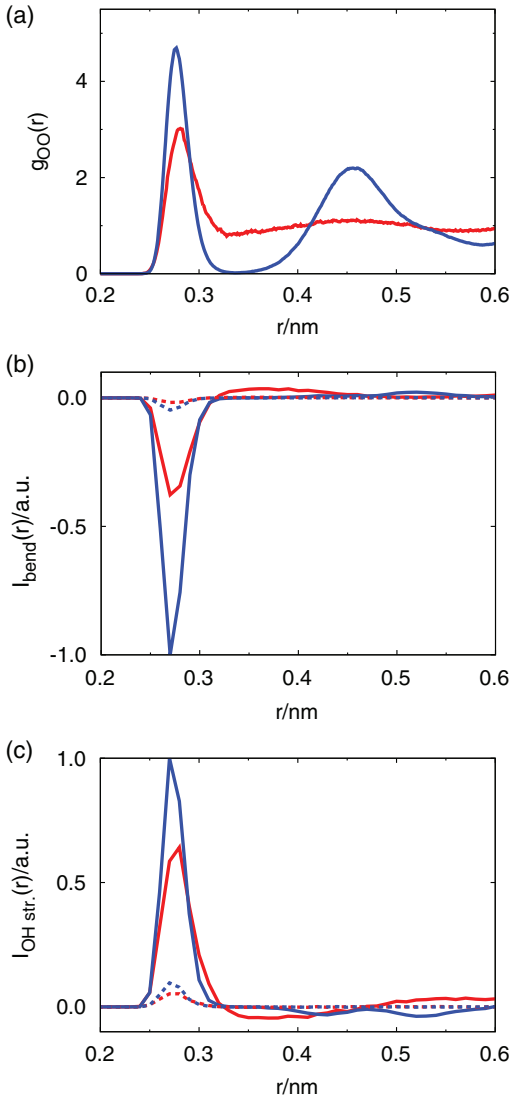

FIG. 5. (a) Oxygen-oxygen radial distribution functions of ice (blue) and liquid water (red). Radial components of the cross term for the HOH bend (panel (b)) and the OH stretch (panel (c)). The solid and dotted lines trace the first and second term of Eq. (11), whereas blue (red) lines denote the results for ice (liquid water).

of the central molecule and the induced dipole moment of the HB acceptor molecule is larger than that of the HB donor molecule both in ice and liquid water. The wide distribution of the anti-correlation is due to the sensitivity of the induced dipole moment of the HB acceptor molecule to the OH stretch of the central molecule as shown in the inset of Fig. 6.

We will now discuss the molecular picture of the anti-correlation between the permanent dipole moment of the central molecule and the induced dipole moment of its HB acceptor molecules. The distribution of the HOH angle in ice and liquid water is centered around 106° and the intermolecular oxygen-oxygen-oxygen angle is around 109°. When the HOH angle of the central molecule decreases, the permanent dipole moment of the central molecule becomes larger (Fig. 7, upper panel). In addition, the distance between the oxygen atom of the HB acceptor molecule and the hydrogen atom of the central molecule becomes longer. Thus, the induced dipole moment of the HB acceptor molecule decreases

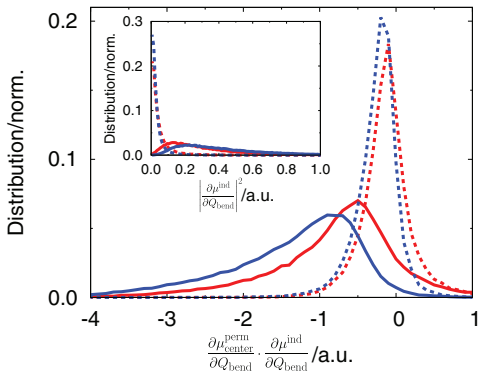

FIG. 6. Distributions of the correlation between the permanent dipole moment of a central molecule and the induced dipole moment of the molecule in its first hydration shell. Solid (dotted) lines trace the correlation between a central molecule and its HB acceptor (donor) molecule, whereas blue (red) lines denote the results for ice (liquid water). Inset shows the distribution of $|\frac{\partial \mu^{ind}}{\partial Q_{bend}}|^2$ in the first hydration sell. The notation in the inset is the same as in the rest of the figure.

due to the decrease in the electric field from the hydrogen atom of the central molecule. Consequently, the increase in the HOH angle of the central molecule results in the decrease in the permanent dipole moment of the central molecule and the increase in the induced dipole moment of the HB acceptor molecule (Fig. 7, lower panel). It is this variation that causes the anti-correlation between the permanent dipole moment of the central molecule and the induced dipole moment of its HB acceptor. Since the HB network is more disordered and consequently the electric field is weakened in liquid water when compared to ice, the anti-correlation between the permanent dipole moment of the central molecule and the induced dipole moment of the HB acceptor molecule is weaker in liquid water than in ice. As indeed shown in Figs. 8(a) and 8(b), the anti-correlation between $\frac{\partial \mu^{perm}_{center}}{\partial Q_{bend}}$ and $\frac{\partial \mu^{ind}_{acceptor}}{\partial Q_{bend}}$ in ice is stronger than that in liquid water.

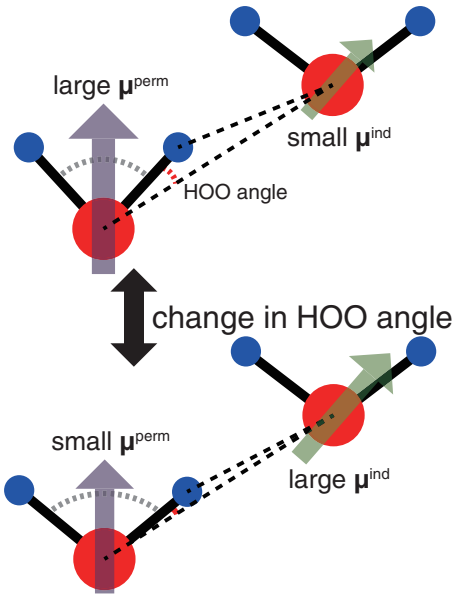

FIG. 7. Scheme showing the origin of the anti-correlation between the permanent dipole moment of a central molecule and the induced dipole moment of its HB acceptor molecule.

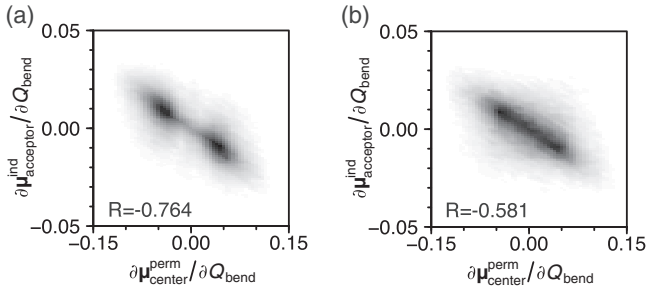

FIG. 8. Correlation of the permanent dipole moment of a central molecule and the induced dipole moment of its HB acceptor molecule in (a) ice with ∼50 000 points and (b) liquid water with ∼40 000 points. The correlation coefficients (R) are also shown.

Similarly, for the OH stretch the permanent dipole moment of the central molecule is larger when its intramolecular OH distance is longer. At the same time, the induced dipole moment of the HB acceptor molecule is larger because of the short intermolecular oxygen-hydrogen distance. Thus, the permanent dipole moment of the central molecule and the induced dipole moment of the HB acceptor molecule show a positive correlation in both ice and liquid water, as shown in Figs. 2(a), 2(b), and 5(c).

All previous results are obtained from the MD trajectories and the normal mode analysis obtained with the TTM3-F potential. To examine the validity of the results obtained from the simulations with TTM3-F potential, we investigated the relation between the $\frac{\partial \mu^{\rm perm}}{\partial Q_{\rm bend}}$ term of the central molecule and the $\frac{\partial \mu^{\rm ind}}{\partial Q_{\rm bend}}$ term of the HB acceptor molecules in pentamer water clusters evaluated via MP2 *ab initio* calculations. The correlations between those two terms calculated for pentamers with the TTM3-F potential and MP2 are shown in Fig. 9. The

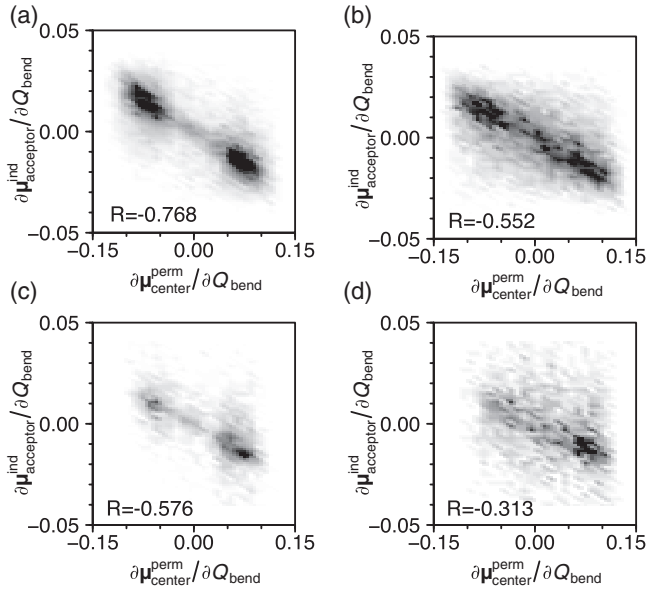

FIG. 9. Correlation of the permanent dipole moment of a central molecule and the induced dipole moment of its HB acceptor molecule from water pentamer clusters extracted from the ice and liquid water trajectories. (a) Ice and (b) liquid water using TTM3-F potential with ∼10 000 points, (c) ice and (d) liquid water based on MP2 calculations with ∼3000 points. The correlation coefficients (R) are also shown.

comparison suggests that the results obtained from the MP2 calculations and with the TTM3-F potential are in excellent agreement in clearly documenting the strong anti-correlation for pentamers taken from ice and a weaker anti-correlation in those extracted from liquid water simulations. This further justifies the results and conclusions reached by the analysis of the trajectories obtained with the TTM3-F potential.

V. CONCLUSIONS

The difference in the IR intensities of the HOH bend between ice and liquid water was investigated using the TTM3-F interaction potential, since this potential correctly reproduces the values of the HOH angle and the IR intensity of the HOH bend in ice and liquid water. We decomposed the IR spectra into the components arising from the permanent, induced, and cross terms. We found that the IR intensity of the HOH bend in ice is weakened by the strong anti-correlation between the permanent dipole moment of a molecule and the induced dipole moment of its HB acceptor molecule, and furthermore that this anti-correlation is small in liquid water because of the disordered HB structure. This anti-correlation in the HOH bend was confirmed by performing MP2 calculations on water pentamers extracted from the liquid water and ice trajectories, which further confirmed the correct behavior of the TTM3-F potential in reproducing this feature of the spectra.

In contrast to the HOH bend, the OH stretch shows a positive correlation between the permanent dipole moment of a molecule and the induced dipole moment of its HB acceptor. Since the ordered HB structure increases the positive correlation, the IR intensity of the OH stretch in ice is larger than that in liquid water.

The sensitivity of the OH stretch on the underlying HB environment is well established. In this study we demonstrated that the IR intensity of the HOH bend is also sensitive to the HB structure. Since the HOH bend is more delocalized than the OH stretch as shown in terms of the IPR, the properties of the HOH bend would be more strongly dependent on the HB network than for the OH stretch. However, much less is currently known about both the static and dynamic properties of the HOH bend in liquid water and ice. We are currently investigating dynamical properties, such as the frequency fluctuation and energy relaxation of the HOH bend, via the theoretical calculation of the nonlinear response function. We also hope that the current study will fuel interest in future experimental probes aiming at the understanding of the much less known static and dynamic properties of the HOH bend in condensed aqueous environments.

ACKNOWLEDGMENTS

The present study was supported by the Grant-in-Aid for Challenging Exploratory Research (Grant No. 23655020), the Grant-in Aid for Scientific Research (Grant No. 22350013), the Strategic Program for Innovation Research (SPIRE), MEXT, and the Computational Material Science Initiative (CMSI). S.S.X. acknowledges the support of the U.S. Department of Energy (DOE), Office of Basic Energy Sciences, Division of Chemical Sciences, Geosciences, and Biosciences.

Pacific Northwest National Laboratory (PNNL) is a multi-program national laboratory operated for DOE by Battelle. The calculation was carried out using the computing resources at the Research Center for Computational Science in Okazaki.

[1]D. Eisenberg and W. Kauzmann, *The Structure and Properties of Water* (Clarendon, 1969).
[2]I. Ohmine and H. Tanaka, Chem. Rev. **93**, 2545 (1993).
[3]J. E. Bertie, H. J. Labbe, and E. Whalley, J. Chem. Phys. **50**, 4501 (1969).
[4]B. Zelent, N. V. Nucci, and J. M. Vanderkooi, J. Phys. Chem. A **108**, 11141 (2004).
[5]J. E. Bertie and Z. Lan, Appl. Spectrosc. **50**, 1047 (1996).
[6]J. J. Loparo, S. T. Roberts, and A. Tokmakoff, J. Chem. Phys. **125**, 194521 (2006).
[7]J. J. Loparo, S. T. Roberts, and A. Tokmakoff, J. Chem. Phys. **125**, 194522 (2006).
[8]J. B. Asbury, T. Steinel, K. Kwak, S. A. Corcelli, C. P. Lawrence, J. L. Skinner, and M. D. Fayer, J. Chem. Phys. **121**, 12431 (2004).
[9]B. Auer, R. Kumar, J. R. Schmidt, and J. L. Skinner, Proc. Natl. Acad. Sci. U.S.A. **104**, 14215 (2007).
[10]D. Kraemer, M. L. Cowan, A. Paarmann, N. Huse, E. T. J. Nibbering, T. Elsaesser, and R. J. D. Miller, Proc. Natl. Acad. Sci. U.S.A. **105**, 437 (2008).
[11]F. Perakis and P. Hamm, Phys. Chem. Chem. Phys. **14**, 6250 (2012).
[12]F. Mallamace, M. Broccio, C. Corsaro, A. Faraone, D. Majolino, V. Venuti, L. Liu, C. Y. Mou, and S. H. Chen, Proc. Natl. Acad. Sci. U.S.A. **104**, 424 (2007).
[13]S. Ashihara, N. Huse, A. Espagne, E. T. J. Nibbering, and T. Elsaesser, J. Phys. Chem. A **111**, 743 (2007).
[14]J. Lindner, P. Vohringer, M. S. Pshenichnikov, D. Cringus, D. A. Wiersma, and M. Mostovoy, Chem. Phys. Lett. **421**, 329 (2006).
[15]S. Ashihara, S. Fujioka, and K. Shibuya, Chem. Phys. Lett. **502**, 57 (2011).
[16]L. Piatkowski and H. J. Bakker, J. Chem. Phys. **135**, 214509 (2011).
[17]P. Bodis, O. F. A. Larsen, and S. Woutersen, J. Phys. Chem. A **109**, 5303 (2005).
[18]F. Ingrosso, R. Rey, T. Elsaesser, and J. T. Hynes, J. Phys. Chem. A **113**, 6657 (2009).
[19]R. Rey, F. Ingrosso, T. Elsaesser, and J. T. Hynes, J. Phys. Chem. A **113**, 8949 (2009).
[20]A. Bastida, J. Zúñiga, A. Requena, and B. Miguel, J. Chem. Phys. **131**, 204505 (2009).
[21]A. Bastida, J. Zúñiga, A. Requena, and B. Miguel, J. Chem. Phys. **136**, 234507 (2012).
[22]A. Kandratsenka, J. Schroeder, D. Schwarzer, and V. S. Vikhrenko, J. Chem. Phys. **130**, 174507 (2009).
[23]W. S. Benedict, N. Gailar, and E. K. Plyler, J. Chem. Phys. **24**, 1139 (1956).
[24]I. C. Baianu, N. Boden, D. Lightowlers, and M. Mortimer, Chem. Phys. Lett. **54**, 169 (1978).
[25]M. A. Floriano, D. D. Klug, E. Whalley, E. C. Svensson, V. F. Sears, and E. D. Hallman, Nature (London) **329**, 821 (1987).
[26]S. S. Xantheas, J. Chem. Phys. **102**, 4505 (1995); S. S. Xantheas and T. H. Dunning, J. Chem. Phys. **99**, 8774 (1993).
[27]Y. A. Mantz, F. M. Geiger, L. T. Molina, M. J. Molina, and B. L. Trout, J. Chem. Phys. **113**, 10733 (2000).
[28]J. Jeon, A. E. Lefohn, and G. A. Voth, J. Chem. Phys. **118**, 7504 (2003).
[29]G. S. Fanourgakis and S. S. Xantheas, J. Chem. Phys. **124**, 174504 (2006).
[30]C. J. Burnham and S. S. Xantheas, J. Chem. Phys. **116**, 5115 (2002); G. S. Fanourgakis and S. S. Xantheas, J. Phys. Chem. A **110**, 4100 (2006).
[31]G. S. Fanourgakis and S. S. Xantheas, J. Chem. Phys. **128**, 074506 (2008).
[32]S. Habershon, G. S. Fanourgakis, and D. E. Manolopoulos, J. Chem. Phys. **129**, 074501 (2008).
[33]F. Paesani, S. S. Xantheas, and G. A. Voth, J. Phys. Chem. B **113**, 13118 (2009).
[34]J. Liu, W. H. Miller, G. S. Fanourgakis, S. S. Xantheas, S. Imoto, and S. Saito, J. Chem. Phys. **135**, 244503 (2011).
[35]F. Paesani, I. Satoru, and G. A. Voth, J. Chem. Phys. **127**, 074506 (2007).
[36]F. Paesani and G. A. Voth, J. Phys. Chem. B **113**, 5702 (2009).
[37]F. Paesani, S. Yoo, H. J. Bakker, and S. S. Xantheas, J. Phys. Chem. Lett. **1**, 2316 (2010).
[38]S. Saito and I. Ohmine, J. Chem. Phys. **108**, 240 (1998).
[39]H. Partridge and D. W. Schwenke, J. Chem. Phys. **106**, 4618 (1997).
[40]B. T. Thole, Chem. Phys. **59**, 341 (1981).
[41]M. P. Allen and D. J. Tildesley, *Computer Simulation of Liquids* (Oxford University Press, 1991).
[42]A. J. Stone, J. Chem. Theor. Comput. **1**, 1128 (2005).
[43]A. J. Stone, Distributed multipole analysis of gaussian wavefunctions GDMA version 2.2, 2005.
[44]R. A. Kendall, T. H. Dunning, Jr., and R. J. Harrison, J. Chem. Phys. **96**, 6796 (1992).
[45]M. J. Frisch, G. W. Trucks, H. B. Schlegel *et al.*, GAUSSIAN 09, Revision A.1, Gaussian, Inc., Wallingford, CT, 2009.
[46]M. Sharma, R. Resta, and R. Car, Phys. Rev. Lett. **95**, 187401 (2005).
[47]L. Shi, S. Gruenbaum, and J. L. Skinner, J. Phys. Chem. B **116**, 13821 (2012).
[48]M. Cho, G. R. Fleming, S. Saito, I. Ohmine, and R. M. Stratt, J. Chem. Phys. **100**, 6672 (1994).
[49]W. Chen, M. Sharma, R. Resta, G. Galli, and R. Car, Phys. Rev. B **77**, 245114 (2008).